OPEN ACCESS
Journal of Innovative Optical Health Sciences
Vol. 16, No. 4 (2023) 2243002 (8 pages)

DOI: 10.1142/S1793545822430027

World Scientific
www.worldscientific.com

Quantitative tracing of bioprobes by simultaneously monitoring radiative and nonradiative relaxations

Hongjiang Chen*, Xiaoyu Tang†,‡, Guangshuai Nie*, Zhen Wang*, Jia Hu*, Jun Hu*,¶ and Huan Qin†,‡,§,‖

*Department of Orthopaedics,
The First Affiliated Hospital of Shantou University Medical College
Shantou 515041, Guangdong Province, P. R. China

†MOE Key Laboratory of Laser Life Science
& Institute of Laser Life Science
College of Biophotonics, South China Normal University
Guangzhou 510631, P. R. China

‡Guangdong Provincial Key Laboratory of Laser Life Science
College of Biophotonics, South China Normal University
Guangzhou 510631, P. R. China

§Guangzhou Key Lab of Spectral Analysis and Functional Probes
College of Biophotonics, South China Normal University
Guangzhou 510631, P. R. China
¶hjzkmst@126.com
‖qinghuan@scnu.edu.cn

Received 7 April 2022
Accepted 24 April 2022
Published 10 June 2022

Bioprobe based on fluorescence is widely used in biological and medical research due to its high sensitivity and selectivity. Yet, its quantification *in vivo* is complicated and often compromised by the interaction between the fluorophore with the environmental factors, as well as the optical scattering and absorption by the tissue. A high florescence quantum yield and minimal interference by the environment are key requirements for designing an effective bioprobe, and the prerequisitions severely limit the available options. We propose that a comprehensive evaluation of potential bioprobe can be achieved by simultaneously measuring both radiative and nonradiative transitions, the two fundamental and complementary pathways for the energy de-excitation. This approach will not only improve the accuracy of the quantification by catching the information from a broader spectrum of the energy, but also provide additional information of the probe environment that often impacts the balance between the two forms of the energy transition. This work first analyzes the underlying mechanism of the hypothesis. The practical feasibility is then tested by means of simultaneous measurements of photoacoustic signal for the

¶,‖Corresponding authors.

non-radiative and fluorescence for the radiative energy processes, respectively. It is demonstrated that the systematic evaluation of the probe energy de-excitation results in an improved quantitative tracing of a bioprobe in complex environment.

Keywords: Bioprobe; fluorescence; photoacoustic.

1. Introduction

Bioprobes based on fluorescence with high sensitivity and selectivity are widely used in biomedical research.[1–5] *In vivo* monitoring of bioprobes has shown exciting results in localization and dynamics of protein expression, early detection and diagnosis of tumors, and the detection of calcium signal in neurons etc.[6–9] The majority of the current *in vivo* fluorescence imaging techniques measure the changes in radiative relaxation via fluorescence of bioprobes. The results are prone to the variations in the chemical/physiological environment (e.g., pH, ions, protein, solvent polarity, etc.) due to the fluorescence quenching, and by the photon scattering and absorption in tissue before the optical data acquisition. These contribute to significant uncertainties in the accuracy for quantitative work. A high fluorescence quantum and minimal interference from the environment are key factors to be considered in designing an effective bioprobe. These pre-requisites severely limit the options for a potential probe.

It is well known that stimulated emission from an excited fluorescence probe has two major paths: Radiative decay via fluorescence and nonradiative decay via thermal dissipation.[10–13] The radiative and nonradiative transitions occur simultaneously after an excitation, and there is a competitive mechanism between them (see detailed explanation in Sec. 2.1). Given the complementary nature of the two pathways, signal change in one channel may be deduced from the other, if the total is known. Reversely, if the energy from both channels could be captured completely, the summation would more accurately reflect the quantity of the probe. A system that can simultaneously monitor both radiative and nonradiative transitions, thus, will likely provide a more comprehensive evaluation of the probe's behavior, compared to that monitoring either channel alone. Furthermore, as the balance between radiative and nonradiative decay is affected by various environmental factors, the approach may also provide additional information regarding the probe environment.

Presently, nonradiative decay is not usually measured/monitored at the same time with fluorescence, due to technical difficulties. When the excitation is a short pulse (e.g., nanosecond), the heat generated by the nonradiative decay produces an ultrasonic wave via thermoelastic expansion — this is known as the photoacoustic effect.[13–16] The center of the proposed technique is to utilize the same excitation energy for simultaneous monitoring of the radiative and nonradiative relaxations, and ultimately achieving quantitative tracing of bioprobes.

2. Materials and Methods

2.1. *Principle and methods*

The Jablonski diagram[17] (Fig. 1(a), first conceived by Alexander Jablonski in the 1930s), clearly demonstrates the competitive mechanism of the nonradiative transition and radiative transition during a single excitation process. After the probe molecules absorb light energy, electrons transition from the ground state (S_0) to an excited state (S_1), followed by a radiation or nonradiation transition from the excited state to the ground state. The radiative transition process involves fluorescence, delayed fluorescence, or phosphorescence emission, but the proportion of delayed fluorescence and phosphorescence is minimal and negligible. The nonradiative transition process includes vibrational relaxation, internal transfer, intersystem crossing, and external transfer, all of which release energy in the form of heat, an energy source for photoacoustic effects.

When a bioprobe is irradiated by a short pulse laser, the detected fluorescence intensities FI from the probe can be written as follows[18,19]:

$$F_I = AF\varepsilon(\lambda)C\eta, \tag{1}$$

where A is the system transfer function connected fluorescence detection and total fluorescence energy, which is a constant in the same system. F is the laser pulse energy density (J/cm^2). $\varepsilon(\lambda)$ is the molar absorption coefficient of the probe at the excitation wavelength. C is the concentration of the probe. η is the fluorescence quantum yields of the probe. In this work, we assume that the absorption coefficient of the probe affected by environmental factors is negligible.

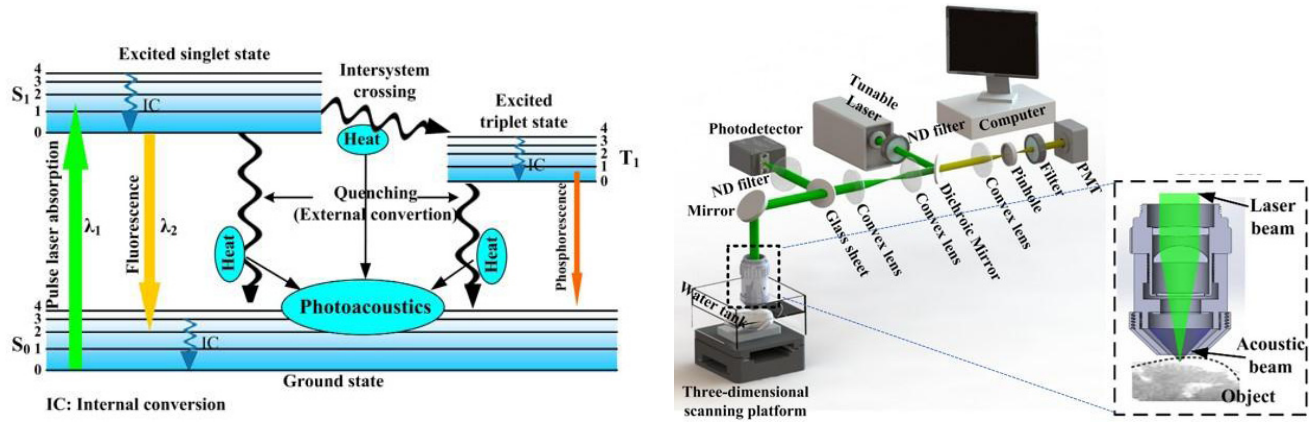

(a) (b)

Fig. 1. (a) The Jablonski diagram indicates the complementarity of photoacoustic and fluorescence signals. (b) The schematic diagram of photoacoustic-fluorescent complementary imaging system. The fluorescent and photoacoustic signals generated during a single excitation process can be simultaneously detected. PL imaging: Fluorescence imaging; PA imaging: Photoacoustic imaging.

To eliminate the effect of fluorescence quantum yield η on the total evaluation of the probe concentration, an intermediate coefficient M is traduced, $M = AF\varepsilon(\lambda)$. Equation (1) becomes $F_I = MC\eta$, M can be titrated from a known concentration C_0 and the corresponding fluorescence intensity at the concentration. η_0 is the fluorescence quantum yields of the probe at C_0.

$$M = \frac{F_{I0}}{C_0\eta_0}, \tag{2}$$

where C_0 is a known concentration. η_0 is the fluorescence quantum yields of the probe at the known concentration, F_{I0} is the fluorescence intensities of the probes at the known concentration.

If the excitation light is a short pulse, then the heat generated during nonradiative decay produces an ultrasonic thermoelastic wave via the thermoelastic expansion. The photoacoustic amplitudes P can be expressed as follows[13,18,19]:

$$P = BF\varepsilon(\lambda)\Gamma C(1-\eta). \tag{3}$$

Here, B is the system of photoacoustic channel transfer function connected photoacoustic detection and total photoacoustic energy. F is optical fluence (J/cm^2). $\varepsilon(\lambda)$ is the molar absorption coefficient of the probe at the excitation wavelength. Γ is the Grüneisen coefficient (nearly constant at room temperature). To simplify Eq. (3), N as an intermediated coefficient is introduced, it is defined as $N = BF\varepsilon(\lambda)\Gamma$, thus Eq. (3) becomes $P = NC(1-\eta)$. Thus N can be calculated as follows:

$$N = \frac{P_0}{C_0(1-\eta_0)}, \tag{4}$$

where C_0 is a known concentration. η_0 is the fluorescence quantum yields of the probe at the known concentration, P_0 is the photoacoustic amplitudes of the probes at the known concentration.

Given the complementary nature of fluorescence and photoacoustics from the probes in a single excitation process, supposing that the detected fluorescence and photoacoustic signal are from the same region and there are no other physical and chemical loss, the sum of the energy from the two channels could be used for quantification of the probes. According to Eqs. (1)–(4), the quantification of the probe can be expressed as follows:

$$\frac{F_I}{M} + \frac{P}{N} = C\eta + C(1-\eta) = C. \tag{5}$$

Equation (5) shows that, in an ideal situation, the fluorescence, and photoacoustic signals from the same probes resulted from a single excitation could be used for quantification of the probes without being affected by the fluorescence quantum yield fluctuation.

To test the technical feasibility of the simultaneous monitoring of the radiative and nonradiative signals, a photoacoustic-fluorescence imaging (PA-FLI) system has been developed (Fig. 1(b)). A pulsed laser beam is expanded and then refocused onto the sample through an objective lens.

The photoacoustic signal generated in the sample is received by an ultrasonic transducer beneath the objective lens, while the fluorescence is simultaneously collected by the objective lens and detected with a photomultiplier (PMT) tube through a dichroic lens and filters. A silicon photodiode monitors and calibrates the intensity of the excitation light. The samples position and the corresponding data PA-FLI system has been successfully constructed and can be used for experimental studies.

2.2. *Materials*

Rhod-2, Atto 680 were purchased from Bridgen biotechnology Co. Ltd (Beijing, China). Tryptophan was purchased from Sigma-Aldrich (Beijing, China). Since all the chemicals were analytical grade and were used without further purification, the high-purity deionized water (resistance $> 18\,\mathrm{M}\Omega$ cm) is used throughout. Neuroblastoma (SH-SY5Y) was obtained from the Cell Culture Center of SunYat-sen University (Guangzhou, China).

The optical absorbance of Atto 680 in the aqueous solution in the absence and presence of tryptophan was investigated by UV/visible absorption spectra (Lambda-35 UV/visible spectrophotometer, Perkin-Elmer, MA, USA). Fluorescence spectra of Atto 680 in the absence and presence of tryptophan were investigated by an LS-55 fluorescence spectrophotometer (Perkin-Elmer).

Cell Culture: Neuroblastoma (SH-SY5Y) cells in Eagle's minimal essential medium. The media were supplemented with 10% fetal bovine serum and 1% penicillin-streptomycin, in 5% CO_2, 95% air at 37°C in a humidified incubator.

Photoacoustic-fluorescent imaging system: The experimental setup was shown in Fig. 1(b). A tunable pulsed laser with a repetition rate of 20 Hz and a pulse width of 4 ns (Nd:YAG Surelight-II-20 connected to Surelite OPO Plus, Spectral tuning range 675–1000 nm, Continuum) was used as the light source. The light through scan lens and tube lens was then focused by the objective lens to irradiate the tested samples. The average energy density of the laser at the wavelengths used in this study was set to be $< 20\,\mathrm{mJ}\cdot\mathrm{cm}^{-2}$ at the target site. The ultrasonic transducer (Doppler Electronic Technologies Co., Ltd., China) with center frequency of 10 MHz and −6 dB bandwidth of 100% was used to receive the PA signals generated by the tested samples. The fluorescence was collected by the objective. The fluorescence through the dichroic mirror and filter was detected by PMT, ultimately. The PA signals and the fluorescence signals were recorded by the computer through a dual-channel data acquisition card. The sampling rate of the data acquisition card was 200 Msamples/S. A 2D scanning stage was driven by computer-controlled ultrasonic motors. A silicon photodiode (ET 2000, Electro-Optics Technology, Inc., Traverse City, USA) was used to monitor and calibrate the intensity and stability of the laser beam. A computer controls an ultrasonic motor to move the samples and analyzes the photoacoustic and fluorescent signals generated at each scan point in real-time. Fluorescent and photoacoustic images within the region of interest can then be obtained, simultaneously.

3. Results and Discussion

In order to demonstrate that the PA-FLI has been built successfully, we did test experiments. Neuroblastoma cells (SH-SY5Y) were labeled with calcium probe (Rhod-2). The PA-FLI system is used to image the labeled neuroblastoma cells simultaneously. The image is shown in Fig. 2. The experimental results verified that a complementary imaging system of PA-FLI system with the same excitation source was successfully constructed and could be used for experimental research.

To experimentally demonstrate that the combined fluorescence and photoacoustic signals in a single excitation process provide a superior means to quantify the probes, Common dyes (Atto 680) were tested as examples. Efficient photoinduced electron transfer (PET) can occur between the first excited singlet state of organic fluorophores and the ground-state of natural amino acids. To demonstrate that probe fluorescence could be affected by the environmental factors, a fluorescence quencher, tryptophan of various concentrations was introduced into the Atto 680 solution and the corresponding fluorescence emission spectra acquired (Fig. 3(a)). With an unvaried [Atto 680], fluorescence intensity decreased as the [tryptophan] escalated, expected as the quencher inserting its effect. (Fig. 3(a) insert).

At the same pulsed laser excitation, the PA-FLI system simultaneously detected the fluorescence and photoacoustic signals of Atto 680. The results show that as the concentration of the florescence

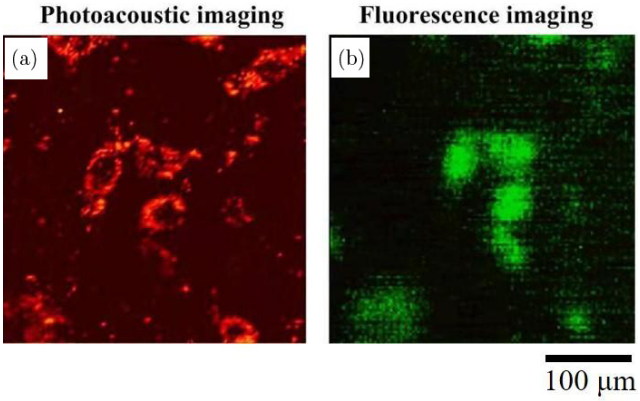

Fig. 2. Photoacoustic (a) and fluorescence (b) images of neuroblastoma cells (SH-SY5Y) labeled with calcium probe (Rhod-2).

quencher Tryptophan increases, the Atto 680 fluorescence signals reduced and the photoacoustic signals increased, correspondently (Figs. 3(b) and 3(c)). In this particular case, the fluorescence or photoacoustic intensity of the probes was sharply changed due to fluorescence quenching. Clearly, neither fluorescence nor photoacoustic signal alone would not accurately reflect the actual quantity of the probe. Yet, by combining the simultaneously acquired fluorescence and photoacoustic in Eq. (5),

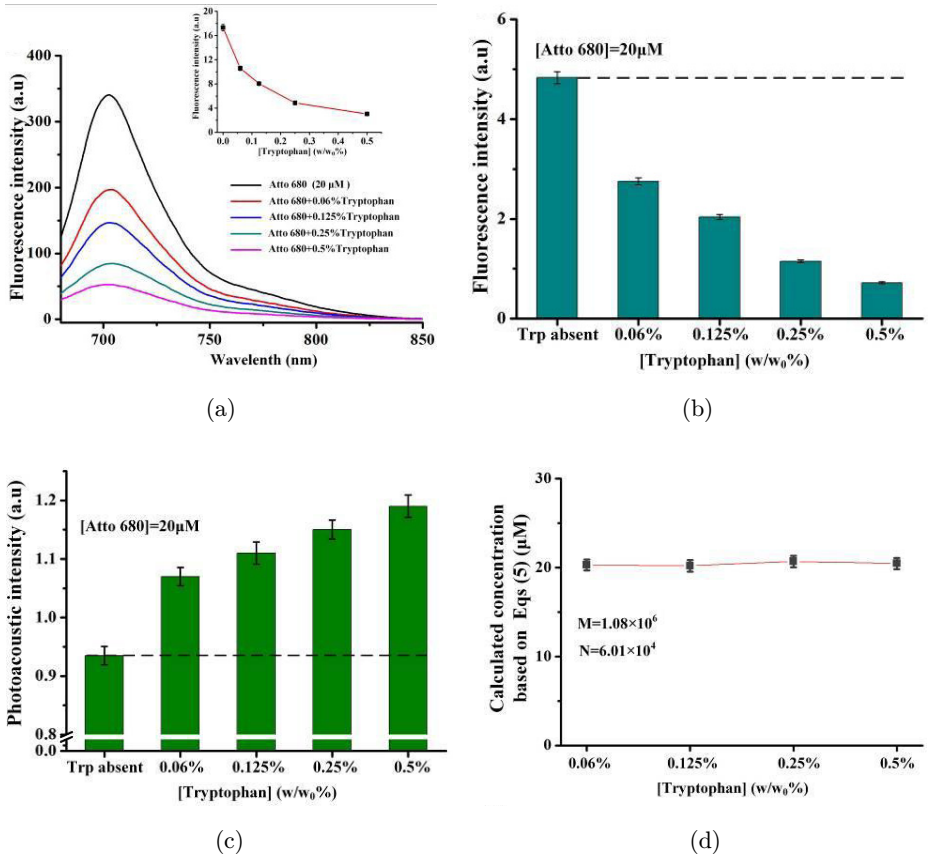

Fig. 3. Dynamic process with induced interference shows the reliability of the quantitative measurement. The photoacoustic and fluorescence nature of the representative dye (Atto 680) with and without influence of environmental factor (tryptophan). (a) The fluorescence spectra of Atto 680 in aqueous solutions with different tryptophan concentrations. Quantitative Atto 680 fluorescence (b) and photoacoustic signal (c) intensity detected by the photoacoustic-fluorescence imaging (PA-FLI) system at aqueous solutions with different tryptophan concentrations. (d) The quantification of the Atto 680 calculated by Eq. (5). According to the fluorescence and photoacoustic signal in a single excitation process (excited at 680 nm), data are shown mean ± SD ($n = 3$).

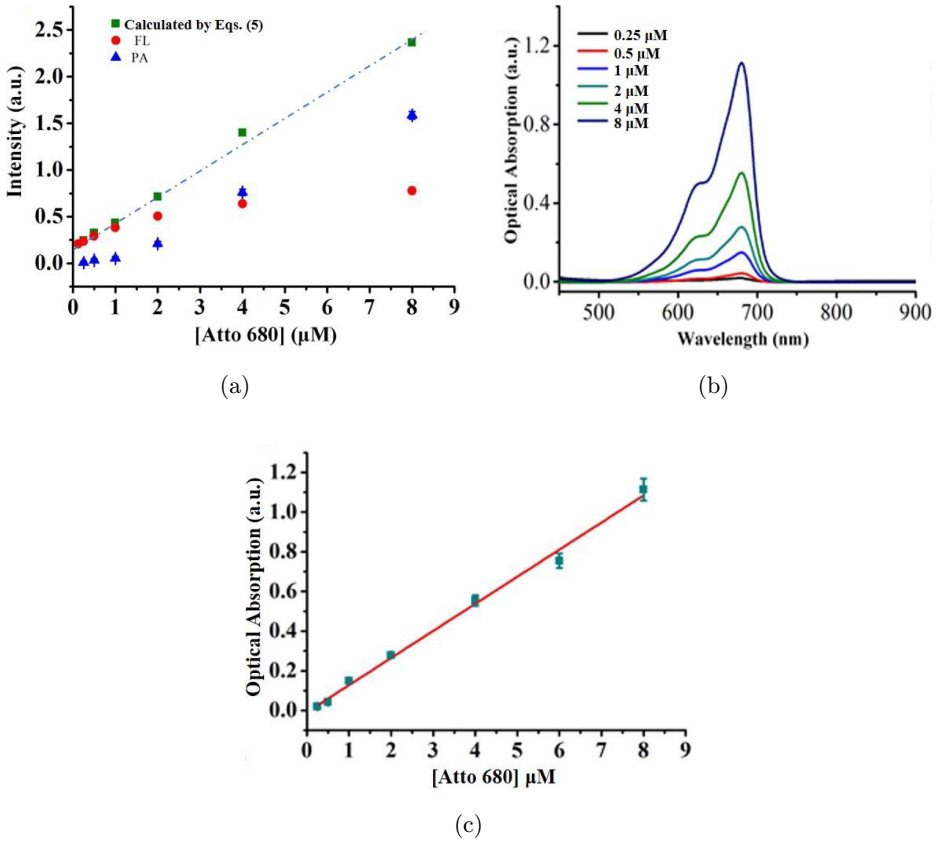

Fig. 4. (a) Fluorescence (red dot) and photoacoustic (blue triangle) signals of different Atto 680 concentrations (0.25–8 μM). The quantification of Atto 680 according to Eq. (5) (green square). The error bars represent standard deviations of three separate measurements. (b) Optical absorption spectrum of different Atto 680 concentrations (0.25–8 μM). (c) Optical absorption value at 680 nm of different Atto 680 concentrations (0.25–8 μM). Data are shown mean $\pm$ SD ($n = 3$).

a more accurate quantification of the probe, independent of the fluorescence quenching efficiency, could be achieved (Fig. 3(d)).

Fluorescence quenching usually occurs when the fluorescence probe concentration is too high.[20] Fluorescence quenching resulted in inaccurate measurement of probe concentration by the fluorometric method. Figure 4(a) shows that the fluorescence intensity was no longer linearly related to the Atto 680 concentration due to the fluorescence quenching phenomenon. The relationship between photoacoustic signal intensity and probe concentration is not linear. Therefore, when the probe gathers to a certain concentration and fluorescence quenching occurs, the single photoacoustic or fluorescence signal cannot accurately reflect the concentration of the probe. Due to the complementary relationship between photoacoustic and fluorescent signals, one increases and the other decreases. Using Eq. (5), combined with photoacoustic and fluorescence signals, the probe can still be quantified (Fig. 4(a), green square). If the quenching effect of fluorescence does not cause changes in the absorption spectrum of the probe, it may be possible to quantify the probe by measuring its absorption (Figs. 4(a) and 4(b)). However, it is difficult to accurately and noninvasively measure the optical absorption value of the research object *in vivo*. The simultaneous measurement of photoacoustic and fluorescence signals during the same excitation process by PA-FLI system could be an accurate method to quantify probe concentration *in vivo*.

The simultaneous measurement of photoacoustic and fluorescence signals of the bioprobes by PA-FLI system has the potential for quantitative tracing of bioprobes. However, at present, our theoretical model has not considered the influence of actual light transmission or acoustic transmission loss on the measurement accuracy. We hope to add the loss in the conduction process as a parameter to the model in the next study. The method presented in this paper is currently only suitable for adaptation

in the point excitation mode. The point scanning mode limits the imaging speed of the PA-FLI system. The current system still uses the mechanical scanning mode, and the imaging speed is still relatively slow, so it is difficult to realize the real-time scanning of the region of interest. There is still a limitation to tracking probes that move or diffuse rapidly. The application of our method to small animal imaging requires further improvement in imaging speed and further consideration of the impact of measurement results on the loss of fluorescence and ultrasound transmission.

4. Conclusions

In this work, we developed a method to accurately quantify fluorescent probes. The method quantifies the probe by simultaneous measuring of photoacoustic signal for the nonradiative and fluorescence for the radiative energy processes, respectively. The experimental results show that when the fluorescence quantum efficiency of the probe is affected by environmental factors, the fluorescence probe can be accurately quantified by integrating photoacoustic and fluorescence signal intensity through Eq. (5). In addition, when fluorescence quenching occurs due to high concentration of probes, our proposed method can still accurately quantify the probes. The systematic evaluation of the probe energy de-excitation could improve quantitative tracing of a bioprobe in complex environment.

Conflict of Interest

The authors declare no conflict of interest.

Acknowledgments

This research was supported by the National Natural Science Foundation of China (62075066); Guangdong Basic and Applied Basic Research Foundation (2021A1515011285, 2019A1515010800). Major Project under the Science and Technology Development Scheme of Guangdong Province (210715106900918, [2020]53-129). Shantou Science and Technology Plan Medical and Health Category Project (211114216492935).

References

1. S. K. Ghosh, P. Kim, X. A. Zhang, S. H. Yun, A. Moore, S. J. Lippard, Z. Medarova, "A novel imaging approach for early detection of prostate cancer based on endogenous zinc sensing," *Cancer Res.* **70**, 6119–6127 (2010).
2. J. Ast, A. Arvaniti, N. H. F. Fine, D. Nasteska, F. B. Ashford, Z. Stamataki, Z. Koszegi, Z. Bacon, Z. Jones, M. A. Lucey, S. Sasaki, D. I. Brierley, B. Hastoy, A. Tomas, G. D'Agostino, F. Reimann, F. C. Lynn, C. A. Reissaus, A. K. Linnemann, E. D'Este, D. Calebiro, S. Trapp, K. Johnsson, T. Podewin, J. Broichhagen, D. J. Hodson, "Super-resolution microscopy compatible fluorescent probes reveal endogenous glucagon-like peptide-1 receptor distribution and dynamics," *Nat. Commun.* **11**, 467 (2020).
3. T. Egawa, K. Hirabayashi, Y. Koide, C. Kobayashi, N. Takahashi, T. Mineno, T. Terai, T. Ueno, T. Komatsu, Y. Ikegaya, N. Matsuki, T. Nagano, K. Hanaoka, "Red fluorescent probe for monitoring the dynamics of cytoplasmic calcium ions," *Angew. Chem. Int. Ed. Engl.* **52**, 3874–3877 (2013).
4. Z. C. Liu, X. Jing, S. Zhang, Y. Tian, "A copper nanocluster-based fluorescent probe for real-time imaging and ratiometric biosensing of calcium ions in neurons," *Anal. Chem.* **91**, 2488–2497 (2019).
5. H. Li, Q. Yao, F. Xu, N. Xu, R. Duan, S. Long, J. Fan, J. Du, J. Wang, X. Peng, "Imaging γ-Glutamyltranspeptidase for tumor identification and resection guidance via enzyme-triggered fluorescent probe," *Biomaterials* **179**, 1–14 (2018).
6. Y. An, W. Chang, W. Wang, H. Wu, K. Pu, A. Wu, Z. Qin, Y. Tao, Z. Yue, P. Wang, Z. Wang, "A novel tetrapeptide fluorescence sensor for early diagnosis of prostate cancer based on imaging Zn^{2+} in healthy versus cancerous cells," *J. Adv. Res.* **24**, 363–370 (2020).
7. X. Li, X. Wang, X. Zhang, M. Zhao, W. L. Tsang, Y. Zhang, R. G. Yau, L. S. Weisman, H. Xu, "Genetically encoded fluorescent probe to visualize intracellular phosphatidylinositol 3,5-bisphosphate localization and dynamics," *Proc. Natl. Acad. Sci. USA* **110**, 21165–211770 (2013).
8. S. Lu, G. Li, Z. Lv, N. Qiu, W. Kong, P. Gong, G. Chen, L. Xia, X. Guo, J. You, Y. Wu, "Facile and ultrasensitive fluorescence sensor platform for tumor invasive biomaker β-glucuronidase detection and inhibitor evaluation with carbon quantum dots based on inner-filter effect," *Biosens. Bioelectron.* **85**, 358–362 (2016).
9. T. Egawa, K. Hanaoka, Y. Koide, S. Ujita, N. Takahashi, Y. Ikegaya, N. Matsuki, T. Terai, T. Ueno, T. Komatsu, T. Nagano, "Development of a far-red to near-infrared fluorescence probe for calcium ion and its application to multicolor neuronal imaging," *J. Am. Chem. Soc.* **133**, 14157–14159 (2011).

10. Y. Lao, D. Xing, S. H. Yang, L. Z. Xiang, "Noninvasive photoacoustic imaging of the developing vasculature during early tumor growth," *Phys. Med. Biol.* **53**, 4203–4212 (2008).
11. S. Yang, D. Xing, Q. Zhou, L. Z. Xiang, Y. Q. Lao, "Functional imaging of cerebrovascular activities in small animals using high-resolution photoacoustic tomography," *Med. Phys.* **34**, 3294–3301 (2007).
12. H. F. Zhang, K. Maslov, G. Stoica, L. V. Wang, "Functional photoacoustic microscopy for high-resolution and noninvasive *in vivo* imaging," *Nat. Biotechnol.* **24**, 848–851 (2006).
13. L. V. Wang, S. Hu, "Photoacoustic tomography: *In vivo* imaging from organelles to organs," *Science* **335**, 1458–1462 (2012).
14. B. Yan, H. Qin, C. Huang, C. Li, Q. Chen, D. Xing, "Single-wavelength excited photoacoustic-fluorescence microscopy for *in vivo* pH mapping," *Opt. Lett.* **42**, 1253–1256 (2017).
15. Q. Yu, S. Huang, Z. Wu, J. Zheng, X. Chen, L. Nie, "Label-free visualization of early cancer hepatic micrometastasis and intraoperative image-guided surgery by photoacoustic imaging," *J. Nucl. Med.* **61**, 1079–1085 (2020).
16. C. G. Lou, L. M. Nie, D. Xu, "Effect of excitation pulse width on thermoacoustic signal characteristics and the corresponding algorithm for optimization of imaging resolution," *J. Appl. Phys.* **110**, 083101 (2011).
17. A. Jablonski, "Efficiency of anti-Stokes fluorescence in dyes," *Nature* **131**, 839–840 (1933).
18. L. Gao, C. Zhang, C. Li, L. V. Wang, "Intracellular temperature mapping with fluorescence-assisted photoacoustic-thermometry," *Appl. Phys. Lett.* **102**, 193705 (2013).
19. Y. Wang, L. V. Wang, "Förster resonance energy transfer photoacoustic microscopy," *J. Biomed. Opt.* **17**, 086007 (2012).
20. L. Nie, D. Xing, S. Yang, "*In vivo* detection and imaging of low-density foreign body with microwave-induced thermoacoustic tomography," *Med. Phys.* **36**, 3429–3437 (2009).